uncertainty arises from the proximity of this peak to the more intense C(1)–B(5) peak. In the microwave study the consistency of results is excellent for those bond lengths, which are unaffected either by an atom being on the principal axis or by a large rotation of the axes upon isotopic substitution,[5] such as C(2)–B(3). The bond distance, C(2)–B(3), from the microwave structure is 1.605 ± 0.005 Å.

For the B(5) atom, which is near the principal *a* axis, its *b* and *c* coordinates are not easily determined by microwave spectroscopy. The B(5)–B(4), 1.721 ± 0.015 Å, and B(5)–C(1), 1.627 ± 0.015 Å, have comparatively large uncertainties. The corresponding bond lengths determined by electron diffraction are 1.723 ± 0.008 and 1.621 ± 0.004 Å. When both rotational constants and diffraction intensities are simultaneously available, the gas-phase structure can be more accurately determined and resolve the problem of closely spaced internuclear distances so often encountered in electron diffraction.

The molecular structure of the carbahexaborane(7) has been established as a distorted octahedron, Figure 5. Referring to Table II many of the structural parameters for the 1,2-$B_4C_2H_6$, 1,6-$B_4C_2H_6$, and CB_5H_7 are quite similar. As in the 1,2-$B_4C_2H_6$ and 1,6-$B_4C_2H_6$ the $qM(q)$ curves are all comparable out to $90q$ (Å^{-1}). Onak et al. have noted the common octahedral geometry found for these three carboranes is reflected in the similar range of chemical shift values obtained in the ^1H and ^{11}B NMR spectra.[8] The most unusual structural feature of CB_5H_7 is the location of the bridging hydrogen. In order to determine a unique structure for CB_5H_7, data were collected to $132q$ (Å^{-1}). We were unable to assign hydrogen positions based on data collected to only $100q$ (Å^{-1}). Figure 7 is a projection of the bridge hydrogen H(7) upon the pseudo-threefold face of the octahedron B(2)B(3)B(6). This is consistent with the ^1H and ^{11}B NMR results found by Onak and "would allow the tautomeric hydrogen to follow a path with little deviation from an appropriately placed imaginary plane just below the equatorial boron atoms." The B(2)–H(7) distance of 1.328 Å and the B(6)-H(7) distance of 1.398 Å are consistent with the boron–hydrogen distance in other bridge bonds. The nearly equivalent distances of H(7) from either B(2), B(3), or B(6) indicates the bridging hydrogen is bound to all three borons, which may account for the very low vibrational amplitude of 0.057 Å for H(7). The value for the bridging hydrogen in pentaborane(9) is 0.085 Å. The placement of the H(7) atom in a position considerably closer to B(6) would then permit tautomeric movement of the bridge hydrogen around the octahedra with intermediate positions at the B(3)–B(6) edges.

In the generation of CB_5H_7 from the corresponding $CB_5H_6^-$, the H^+ would seek the maximum point of electron density on the polyhedral face. Armstrong et al. using self-consistent field molecular orbital calculations on highly symmetrical cage anions, i.e., $B_6H_6^{2-}$, revealed that the electron density builds up inside the cage and reaches a maximum at the center and on the trigonal faces.[20] Since carbon is more electronegative than boron, the H^+ ion would seek out the B(2)B(3)B(6) trigonal face.

Registry No. SF_6, 2551-62-4; 2,3-$B_4C_2H_8$, 21445-77-2; 1,2-$B_4C_2H_6$, 20693-68-9; CB_5H_7, 54423-77-7.

References and Notes

(1) E. A. McNeill, K. L. Gallaher, F. R. Scholer, and S. H. Bauer, *Inorg. Chem.*, **12**, 2108 (1973).
(2) E. A. McNeill and F. R. Scholer, submitted for publication in J. *Mol. Struct.*
(3) R. K. Bohn and M. D. Bohn, *Inorg. Chem.*, **10**, 352 (1971).
(4) V. S. Mastryukov, L. V. Vilkov, A. F. Zhigach, and V. N. Siryatskaya, *Zh. Strukt. Khim.*, **12**, 1081 (1971); **10**, 136 (1969); **7**, 883 (1966).
(5) R. A. Beaudet and R. L. Poynter, *J. Chem. Phys.*, **53**, 1899 (1970).
(6) C. S Cheung and R. A. Beaudet, *Inorg. Chem.*, **10**, 1144 (1971).
(7) R. W. Jotham and D. J. Reynolds, *J. Chem. Soc. A*, 3181 (1971).
(8) E. Groszek, J. B. Leach, G. T. F. Wong, C. Ungermann, and T. Onak, *Inorg. Chem.*, **10**, 2770 (1971).
(9) R. A. Beaudet, paper presented at the Second International Meeting on Boron Chemistry, University of Leeds, Leeds, England, March 1974.
(10) J. R. Spielman and J. E. Scott, *J. Amer. Chem. Soc.*, **87**, 3512 (1965).
(11) S. H. Bauer and K. Kimura, *J. Phys. Soc. Jpn.*, **17**, 300 (1962).
(12) R. L. Hilderbrandt and S. H. Bauer, *J. Mol. Struct.*, **3**, 325 (1969).
(13) Y. Murata, K. Kuchitsu, and M. Kimura, *Jpn. J. Appl. Phys.*, **9**, 591 (1970).
(14) S. H. Bauer, R. R. Karl, and K. L. Gallaher.
(15) W. Harshbarger, G. Lee, R. F. Porter, and S. H. Bauer, *Inorg. Chem.*, **8**, 1683 (1969).
(16) A. L. Andreassen, D. Zebeleman, and S. H. Bauer, *J. Amer. Chem. Soc.*, **93**, 1148 (1971).
(17) A. L. Andreassen and S. H. Bauer, *J. Phys. Chem.*, **76**, 3099 (1972).
(18) $R = |I_{obsd} - I_{calcd}|/|I_{calcd}|$; I_{obsd} is the observed intensity and I_{calcd} is the calculated intensity.
(19) W. C. Hamilton, *Acta Crystallogr.*, **18**, 502 (1965).
(20) D. R. Armstrong, P. G. Perkins, and J. P. Stewart, *J. Chem. Soc. A*, G27 (1973).

Contribution from the Department of Chemistry,
Cornell University, Ithaca, New York 14850

Ion–Molecule Chemistry of BF_3 and HBF_2 in Hydrogen

ROBERT C. PIERCE and RICHARD F. PORTER*

Received September 27, 1974 AIC406782

Comparative proton affinity studies indicate that HBF_2 and BF_3 are protonated by H_3^+ but not by CH_5^+. Boundaries on the proton affinities of these fluoroboranes are set at 5.10 ± 0.40 eV. At low temperatures near 80°K clustering reactions of BF_2^+ occur with formation of the complexes $BF_2{\cdot}H_2^+$ and $BF_2{\cdot}2H_2^+$. In the BF_3–H_2 system a low-temperature complex $BF_3H{\cdot}H_2^+$ is observed. Third-order rate constants for these clustering reactions have been measured. Physical evidence and theoretical calculations indicate that the species $BF_2{\cdot}H_2^+$ formed by a cluster reaction is structurally distinguishable from $H_2BF_2^+$ formed by proton transfer to HBF_2. The species $BF_2{\cdot}2H_2^+$ and $BF_3H{\cdot}H_2^+$ can be treated as four-coordinate structures if each H_2 is counted as one unit three-center bonded to the boron atom.

Introduction

In recent years there has been an increased interest in the kinetic and thermodynamic aspects of proton-transfer reactions in the gas phase. An impetus to this research has been the development of new mass spectrometric techniques including ion cyclotron resonance and chemical ionization which have been used extensively in studies of organic molecules. We have applied the chemical ionization technique to studies of a series of boron hydride molecules and have observed some relationships between basicity (proton affinity) and structure.[1] The original motivation for the experimental work described in the present paper was to obtain a quantitative measure of the basicity of BF_3 which is chemically important as a strong Lewis acid in solution. The experiments have revealed an interesting

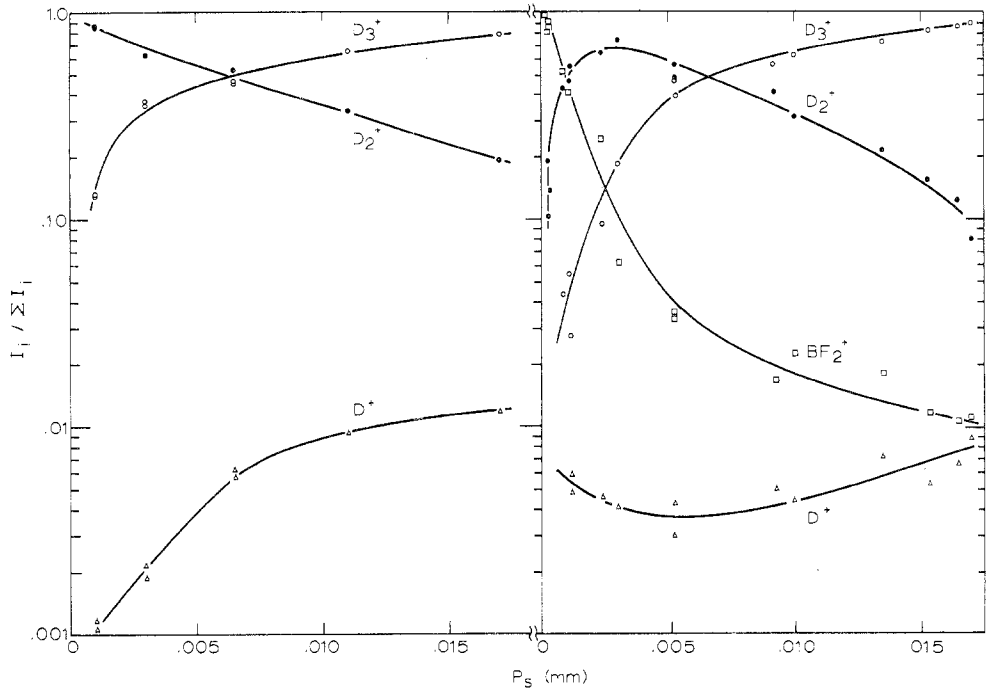

Figure 1. Relative intensities of major ionic species in a D_2 sample (left) and a D_2-condensed BF_3 sample (right) as a function of source pressure for low pressures at 83°K.

ion–molecule chemistry of BF_3 in hydrogen at low temperatures.

Experimental Section

The low-temperature chemical ionization mass spectrometer used in this study has been described previously.[2] Hydrogen and deuterium gases were Matheson prepurified grade. Boron trifluoride was Matheson CP grade purified by standard vacuum techniques. Difluoroborane was prepared by allowing mixtures of boroxine ($H_3B_3O_3$) and boron trifluoride to react.[3] Boroxine was prepared by an explosion reaction of B_2H_6–O_2 mixtures at low pressures.[4] Difluoroborane prepared by this method contained small amounts of BF_3 which were not completely separable by standard fractionation techniques. In addition HBF_2 rapidly disproportionates by the reaction

$$3HBF_2 \rightarrow {}^1/_2B_2H_6 + 2BF_3 \quad (1)$$

To reduce this disproportionation HBF_2 was stored in the condensed phase. The true molar fraction of HBF_2 in a sample, which was nominally pure HBF_2, hence was determined by infrared analyses of the gas samples utilizing the extinction coefficients of the individual components. The methane used in this study was Matheson reagent grade.

In all CI experiments the field strength in the source cavity was maintained at 2.5 V/cm.

BF_3–H_2 Mixtures. Products of ion–molecule reactions occurring in BF_3–H_2 mixtures at a source temperature of 80°K include BF_3H^+, $BF_3H{\cdot}H_2^+$, $BF_2{\cdot}H_2^+$, and $BF_2{\cdot}2H_2^+$. Compositions of the ions were verified by noting the mass effect when H_2 was diluted with D_2 in the reaction mixture. The species BF_3H^+ (protonated BF_3) was observed at source temperatures up to ~300°K in dilute mixtures of H_2–BF_3. The other species were observed only over a short temperature range above 80°K. The vapor pressure of BF_3 at 80°K was determined to be $(1.0 \pm 0.9) \times 10^{-4}$ mm. Consequently, source pressure and composition were adjusted to ensure that the gas phase was below saturation with respect to BF_3. A second mode of operation employed in these studies was that in which a small amount of BF_3 was condensed in the ion source at approximately 80°K and the reagent gas was added through the needle valve in pure form. In this mode the partial pressure of BF_3 was constant within the range of total source pressures investigated (the partial pressure of BF_3 was the equilibrium vapor pressure measured at these temperatures). In Figures 1 and 2 the relative intensities of ions observed in these type of experiments where D_2 served as the reagent gas are presented. In experiments with fixed-composition mixtures the increase in the sum of the $BF_2{\cdot}H_2^+$ and $BF_2{\cdot}2H_2^+$ intensities with decreasing temperature is observed to follow directly the decrease in BF_2^+ intensity (see Figure 3). This leads to defining the stoichiometric relationships

$$BF_2^+ + H_2 \rightarrow BF_2{\cdot}H_2^+ \quad (2)$$

$$BF_2{\cdot}H_2^+ + H_2 \rightarrow BF_2{\cdot}2H_2^+ \quad (3)$$

At low source pressures the origin of BF_2^+ is assumed to be due mainly to electron impact fragmentation of BF_3. As noted in Figure 1 in the limit of zero deuterium pressure BF_2^+ is the major species present. In the BF_3–H_2 experiments at higher source pressures the BF_2^+ intensities are too large to be accounted for exclusively by electron impact of BF_3. Two exothermic processes that may contribute to BF_2^+ production are

$$H^+ + BF_3 \rightarrow BF_2^+ + HF \quad (4)$$

$$H_2^+ + BF_3 \rightarrow BF_2^+ + HF + H \quad (5)$$

From the heats of formation of H^+ (366 kcal/mol),[5] H_2^+ (356 kcal/mol),[5] BF_3 (−271 kcal/mol),[6] BF_2^+ (87 kcal/mol),[6] HF (−65 kcal/mol),[6] and H (52 kcal/mol)[6] we calculate $\Delta H°$ values of −73 and −11 kcal/mol for the respective reactions. By comparison with the blank spectra in Figures 1 and 2 it is obvious that the D_2^+ intensities are approximately of the same relative proportions as in the spectra of samples containing D_2 and BF_3. The D^+ levels are substantially lower in the sample spectra than in the blank spectra. Although a comparative argument of this sort is not absolute, it indicates that reaction 4 is a likely additional source of BF_2^+ at high pressures. The process

$$H_3^+ + BF_3 \rightarrow BF_2^+ + HF + H_2 \quad (6)$$

was also considered as a possible source of BF_2^+. However, the available thermochemical data indicate this process is probably too endothermic to be of any consequence ($\Delta H° \approx 35$ kcal/mol).

Two processes should be considered as probable sources of BF_3H^+. These are

$$BF_3^+ + H_2 \rightarrow BF_3H^+ + H \quad (7)$$

$$H_3^+ + BF_3 \rightarrow BF_3H^+ + H_2 \quad (8)$$

Reaction 8 would appear to be the primary source of BF_3H^+ since the relative intensity of this ion is much higher than would be expected if it were formed only from the small number of BF_3^+ ions produced on electron impact or charge transfer from H_2^+. Thermodynamic considerations indicate that, if reaction 8 is spontaneous in the forward direction, reaction 7 is also spontaneous. By a method of relative comparative cross sections using the EI-scattering ion source design

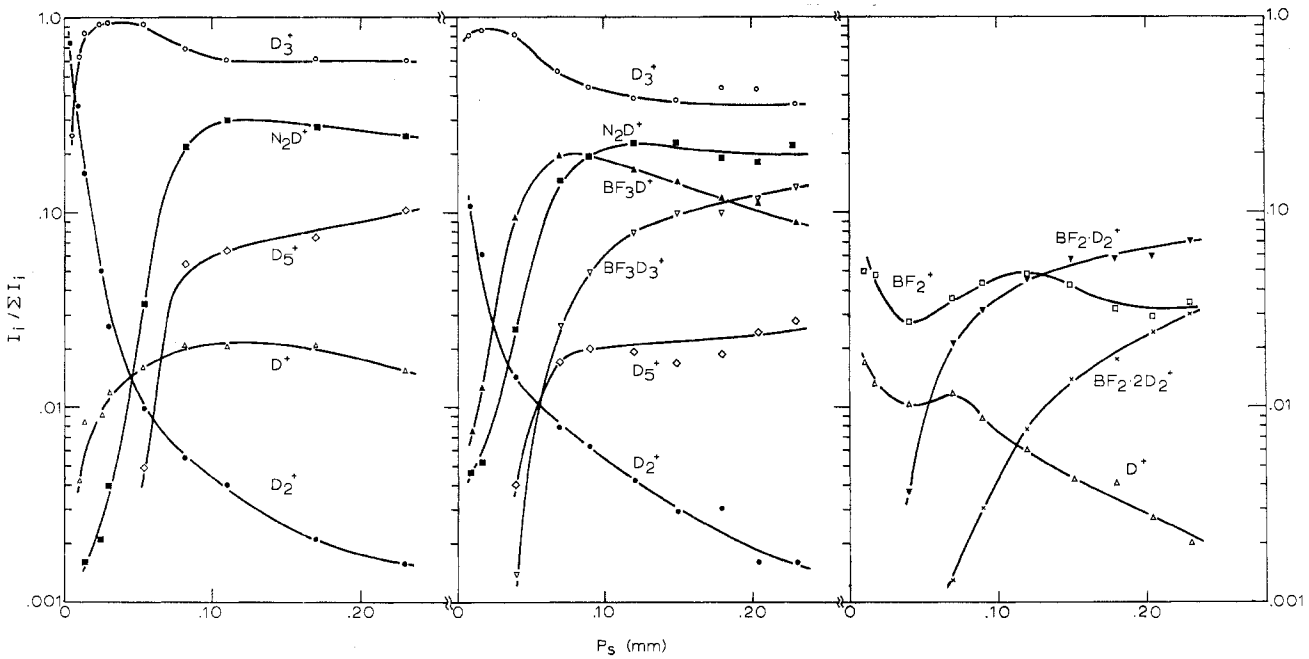

Figure 2. Relative intensities of major ionic species in a D_2 sample (left) and a D_2–condensed BF_3 sample (middle and right) as a function of source pressure at 83°K.

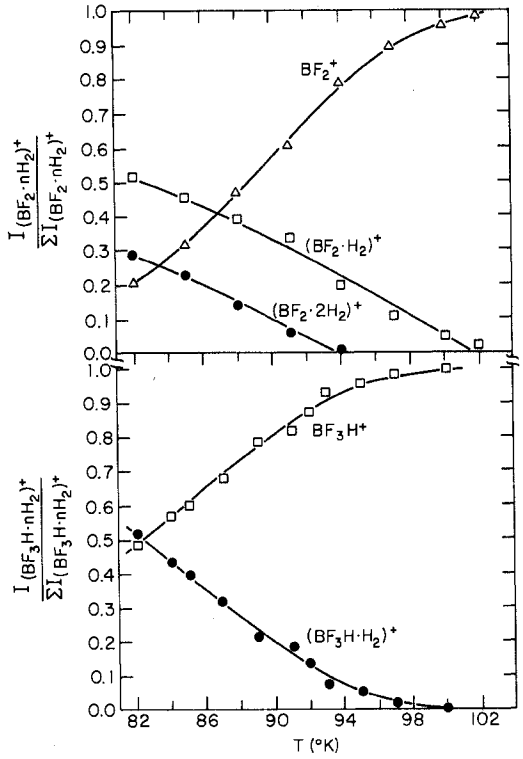

Figure 3. Temperature-dependent ion intensities for 1:2000 (top) and 1:1800 (bottom) BF_3–H_2 mixtures at pressures of 0.20 and 0.18 mm, respectively.

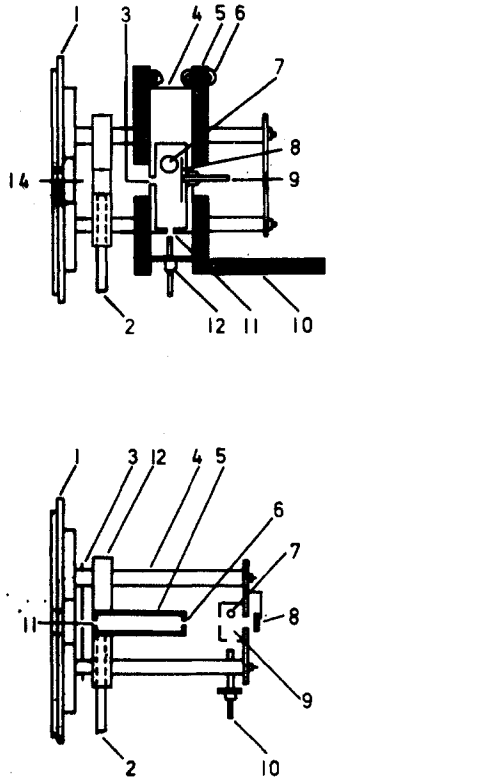

Figure 4. Ion source designs utilized in scattering experiments. Top diagram, conventional low-temperature CI source fitted with scattering chamber: 1, quadrupole mounting plate; 2, scattering chamber gas inlet; 3, CI source ion exit hole; 4, source block; 5, Cu plates; 6, refrigerant coils; 7, gas inlet; 8, Ta repeller; 9, repeller support; 10, refrigerant inlet; 11, electron entrance slit; 12, filament holder and filament; 14, scattering chamber. Bottom diagram, electron impact source fitted with long path length scattering chamber: 1, quadrupole mounting plate; 2, scattering chamber gas inlet; 3, drawout plate; 4, quartz support; 5, scattering chamber; 6, chamber entrance orifice; 7, EI gas inlet; 8, repeller plate; 9, EI chamber; 10, filament holder and filament; 11, scattering chamber exit orifice; 12, scattering chamber support.

illustrated in the lower part of Figure 4, an upper limit on the rate constant for reaction 7 may be established. The rate for reaction 7 was compared with that for the process[6]

$$Ar^+ + H_2 \xrightarrow{k_0} ArH^+ + H \quad k_0 = 1.1 \times 10^{-9}\ cm^3/(molecule\ sec) \qquad (9)$$

utilizing 1.0-eV BF_3^+ and Ar^- ions. The rate constant for reaction 7 was calculated from the relationship

$$\frac{k_1}{k_0} \propto \frac{g_1\sigma_1}{g_0\sigma_0} \propto \frac{I(S_1^+)/I(P_1^+)}{I(S_0^+)/I(P_0^+)} \qquad (10)$$

For small conversions of primary ions to secondary ions and under conditions where the number densities of H_2 in the scattering chamber were identical in both measurements, the value of k_1 was determined

Table I. Chemical Ionization Mass Spectrum of HBF_2 in H_2 at 80°K[a]

Ion	Rel intens, $I_i/\Sigma I_i$	Ion	Rel intens, $I_i/\Sigma I_i$
H^+	0.0134	HBF^+	0.113
H_3^+	0.416	BF_2^+	0.00202
H_5^+	0.107	$BF_2H_2^+$	0.155
$B_2H_5^+$	0.0947	$BF_2H_2 \cdot H_2^+$	0.0445
N_2H^+	0.0528		

[a] $p_s = 0.15$ mm; $HBF_2:H_2 = 1:605$.

Table II. Chemical Ionization Mass Spectrum of HBF_2 in D_2 at 90°K[a]

Ion	Rel intens, $I_i/\Sigma I_i$	Ion	Rel intens, $I_i/\Sigma I_i$
D^+	0.0152	$HClD^+$	0.00610
D_3^+	0.545	BF_2^+	0.00520
D_5^+	0.104	BF_2HD^+	0.0758
N_2D^+	0.0596	$BF_2 \cdot D_2^+$	0.00853
HBF^+	0.0355	$BF_2HD \cdot D_2^+$	0.0140
DBF^+	0.126	$BF_2D_2 \cdot D_2^+$	0.00144

[a] $p_s = 0.23$ mm; $HBF_2:D_2 = 1:1000$.

to be $\leq 4 \times 10^{-11}$ cm³/(molecule sec). The rate constant for reaction 8 may be estimated by evaluation of the data in Figure 2 at the lower source pressures. The respective values for reaction 8 at 83°K are $k(H) = (2 \pm 1) \times 10^{-9}$ cm³/(molecule sec) and $k(D) = (8 \pm 5) \times 10^{-10}$ cm³/(molecule sec). Also in Figure 2 we observe that the intensity of BF_3D^+ becomes large only after D_3^+ achieved its maximum intensity. On the basis of these arguments and measurements, we conclude that reaction 8 is the primary source of BF_3H^+.

The species $BF_3H \cdot H_2^+$ observed at low source temperature is simply interpreted as a condensation product in the reaction

$$BF_3H^+ + H_2 \rightarrow BF_3H \cdot H_2^+ \quad (11)$$

The temperature dependence for this process is illustrated in Figure 3.

HBF_2–H_2 Mixtures. Chemical ionization experiments were conducted with dilute mixtures of HBF_2 in H_2 (D_2) at source temperatures from 80 to 280°K. In the low-temperature regime the major ions of interest are BF_2^+, HBF^+, $BF_2H_2^+$, and $BF_2H_2 \cdot H_2^+$. Ion compositions were also verified by deuterium substitution. The intensity of BF_3H^+ that could have arisen from processes involving BF_3 in the samples was negligible. At temperatures up to 280°K in the HBF_2–H_2 system the origin of $BF_2H_2^+$ by the reaction

$$H_3^+ + HBF_2 \rightarrow BF_2H_2^+ + H_2 \quad (12)$$

seems quite clear. The electron impact spectrum of HBF_2 indicates the absence of a parent ion for this species. This would seem to eliminate the importance of the hypothetical process

$$HBF_2^+ + H_2 \rightarrow BF_2H_2^+ + H \quad (13)$$

which could in principle contribute to the observed $BF_2H_2^+$ intensity. Electron impact fragmentation of HBF_2 leads mainly to BF_2^+ and HBF^+ which are also observed under chemical ionization conditions.

Chemical ionization spectra of mixtures of HBF_2–H_2 and HBF_2–D_2 are indicated in Tables I and II, respectively. Ion intensity–pressure profile data for this system are illustrated in Figure 5. In contrast to observations in the BF_3–H_2 system the species with composition $BF_2H_2^+$ is also detected at temperatures up to 280°K.

Scattering Experiments. In a separate set of experiments product ion species were allowed to interact with collision partners external to the CI source. The ion source configuration employed in these experiments is illustrated in the upper portion of Figure 4. Ions produced at near thermal equilibrium with the reagent gas by CI of HBF_2–H_2 and BF_3–H_2 mixtures were allowed to exit the CI source and enter a scattering chamber maintained at a fixed pressure. The scattering gases included O_2, SO_2, NH_3, and CO. Molecular oxygen appeared to be the best suited for this study due to its low relative mass and zero dipole moment, which kept momentum scattering and ion–dipolar interactions to a minimum. The results of the studies using O_2 are presented in Figure 6. What is noted is that the relative intensity of the $BF_2 \cdot H_2^+$ ion from the BF_3–H_2 sample falls at a faster rate with increasing O_2 density than the other ion species, which are presumably scattered by momentum transfer. This indicates a possible

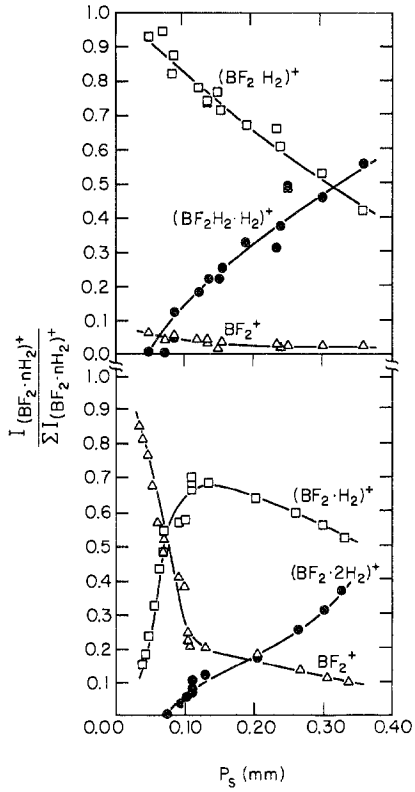

Figure 5. Relative ion intensity–pressure profile for the system $HBF_2:H_2 = 1:605$ (top) and $BF_3:H_2 = 1:2000$ (bottom) at 80° K.

reactive scattering or activation reaction of the form

$$O_2 + BF_2 \cdot H_2^+ \rightarrow BF_2^+ + O_2 + H_2 \quad (14)$$

where the BF_2^+–H_2 bond must be fairly weak. The $BF_2H_2^+$ ion produced by proton transfer in the HBF_2–H_2 system falls in the same relative proportion as the other ions produced in that mixture. This indicates that momentum scattering primarily is effective in this case. The ions H_5^+ and H_7^+, which are also observed in these mixtures and contain weakly bound moieties, appear to exhibit this same type of activation–dissociation behavior. It is concluded that the ion $BF_2 \cdot H_2^+$ produced in the BF_3–H_2 mixtures is an association product of BF_2^+ and H_2 and is structurally different from the $BF_2H_2^+$ species produced by proton transfer in HBF_2–H_2 samples. Further consideration of this point will be made subsequently.

Kinetic Considerations. Reactions 2, 3, and 11 all show the same general type of kinetic behavior with their forward rates decreasing with increasing temperature. Since association processes of this type normally require a third body, as, for example in the formation of H_5^+ from H_3^+ and H_2, the following analysis will be based on the assumption of third-order kinetic behavior. We consider the clustering reactions with eq 2 and 11 renumbered

$$BF_2^+ + 2H_2 \rightarrow BF_2 \cdot H_2^+ + H_2 \quad (15)$$

$$BF_2H_2^+ + 2H_2 \rightarrow BF_2H_2 \cdot H_2^+ + H_2 \quad (16)$$

$$BF_3H^+ + 2H_2 \rightarrow BF_3H \cdot H_2^+ + H_2 \quad (17)$$

Third-order rate constants for these processes were determined at 80°K. Analysis of these constants involves formulation of rate laws of the general type

$$dP^+/dt = k_3 R^+ (p_{H_2})^2 \quad (18)$$

Integration and analysis of these expressions in the region of high E/p described by the Wannier theory of mean ion drift velocity yield[9]

$$k_3 = -[6.80 \times 10^{-4} EkR^2T^3/2\pi d(\alpha\mu)^{1/2} p_{H_2}{}^3] \times \ln\left(\frac{P^+}{P^+ + R^+}\right) \quad (19)$$

where P^+ and R^+ are intensities of product and reactant ion, respectively, E is 8.3×10^{-3} statvolts/cm, α is the polarizibility of H_2,

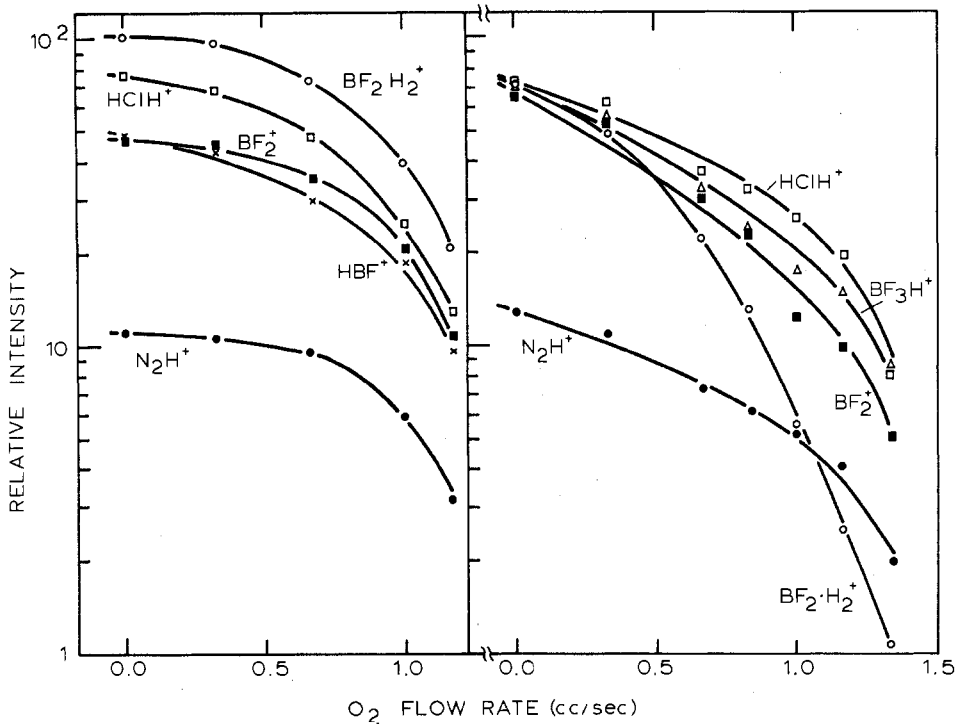

Figure 6. Relative ion intensities *vs.* O_2 flow rate. Sample compositions: left-hand graph, HBF_2:H_2 = 1:200 at p_s = 0.15 mm, T = 120–140°K; right-hand graph, BF_3:H_2 = 1:1000 at p_s = 0.095 mm, T = 85°K. Species: (○) $BF_2 \cdot H_2^+$, (■) BF_2^+; (△) BF_3H^+, (×) HBF^+, (□) $HClH^+$, and (●) N_2H^+.

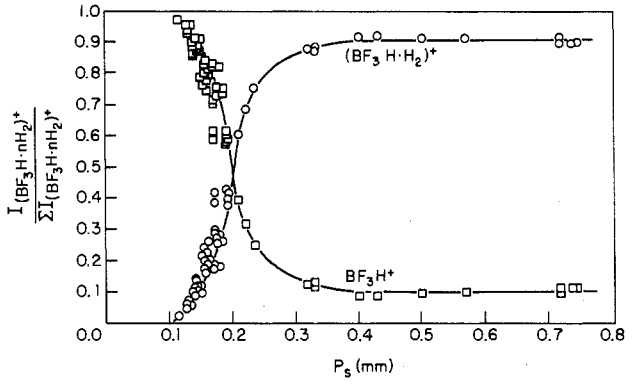

Figure 7. Relative ion intensity–pressure profile for the system BF_3:H_2 = 1:2000 at 87°K.

p is the pressure, d is the drift distance, and μ is the reduced mass of the R^+–H_2 ion–molecule pair in grams. The value of $k_3(17)$ is obtained from data at 80°K similar to that shown at a source temperature of 87°K in Figure 7. The value of $k_3(15)$ is calculated directly from the data for the BF_3–H_2 system shown in Figure 5. For reaction 16 the rate constant $k_3(16)$ was estimated from measurements for the HBF_2–H_2 system under conditions where the initial intensity of $BF_2H_2^+$ was high but where the reaction had proceeded only slightly to the right (Figure 5). The appropriate graphical plots for $k_3(17)$ and $k_3(15)$ are contained in Figure 8. The greater uncertainty present in the $k_3(16)$ plot does not lend itself to effective graphical presentation. The experimental values of $k_3(15)$, $k_3(16)$, and $k_3(17)$ are presented in Table III. The upper limit to the useful source pressure for analysis was dictated by the necessity to remain far below the pressure at which the process of interest began to approach equilibrium (*i.e.*, when the rate of the back-reaction became significant).

Thermodynamic Considerations. In a mixture of HBF_2–CH_4 of composition 1:2000 at 85°K no evidence for protonation of HBF_2 by CH_5^+ is observed at a source pressure of 0.20 mm, indicating that the proton affinity of HBF_2 is less than the PA of CH_4 (130 kcal/mol).[10] For a mixture of 1:2000 BF_3–CH_4 under similar conditions protonation of BF_3 is also not observed. Thus the proton affinities of BF_3 and HBF_3 both lie above the proton affinity of H_2 (4.71 eV reported by D. K. Bohme in a personal communication in ref 7) but

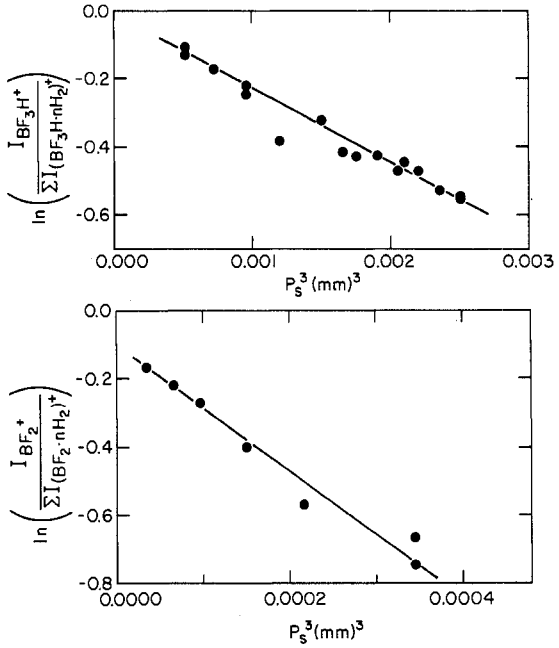

Figure 8. Semilog plots of relative reactant ion intensity *vs.* p_s^3 for the rate constant determinations $k_3(15)$ and $k_3(17)$.

Table III. Third-Order Rate Constants for a Series of Condensation Reactions of H_2 with Boron Fluoride Cations at 80 ± 3°K

Reactions	k_3, cm^2/(molecule sec)^2
$BF_3H^+ + H_2 \rightarrow BF_3H \cdot H_2^+$	$(1.9 \pm 0.2) \times 10^{-28}$
$BF_2^+ + H_2 \rightarrow BF_2 \cdot H_2^+$	$(1.6 \pm 0.3) \times 10^{-27}$
$BF_2H_2^+ + H_2 \rightarrow BF_2H_2 \cdot H_2^+$	$(0.9 \pm 0.5) \times 10^{-28}$

below the proton affinity of CH_4. Hence for the proton addition reaction $H^+ + BF_3 \rightarrow BF_3H^+$ we set $\Delta H° = -117.8 \pm 9.2$ kcal/mol or PA(BF_3) = 5.10 ± 0.40 eV. With the heats of formation of H^+ (366 kcal/mol) and BF_3 (−271 kcal/mol) the $\Delta H_f°(BF_3H^+)$ is then determined to be (−22.8 ± 9.2) kcal/mol. Similarly for the addition

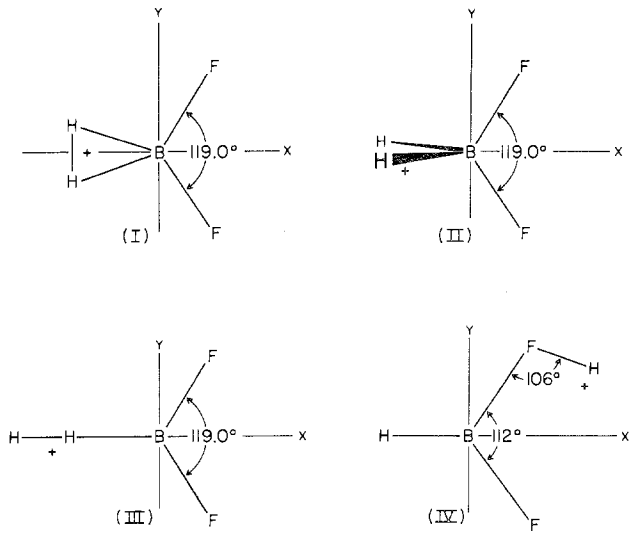

Figure 9. Possible structures for the species $BF_2H_2^+$.

Table IV. Results of CNDO/2 Calculations for the Cation $BF_2H_2^+$

Structure (N)	$E_N - E_I$, kcal/mol	r_{B-F}, Å	r_{B-H}, Å	r_{H-H}, Å	r_{F-H}, Å
I	0.00	1.44	1.37	0.86	
II	2.85	1.44	1.37	0.86	
III	43.20	1.44	1.23	0.78	
IV	−23.39	1.45[a]	1.18		1.03

[a] r_{B-F} in the B-F-H sequence is 1.48 Å.

reaction $H^+ + HBF_2 \rightarrow H_2BF_2^+$ we obtain, using the heat of formation of HBF_2 (−176 kcal/mol), a heat of formation for $H_2BF_2^+$ of 72.2 ± 9.2 kcal/mol.

Structural Considerations. Structural calculations with the CNDO/2 procedure have been successful in predicting the geometrical configurations of simple molecules and ions.[11,12] Recently Olah and coworkers applied the technique to the hypothetical BH_5 molecule and concluded that this species would be isostructural with CH_5^+.[13] The CNDO/2 method has been used as an aid in ranking a series of $BF_2H_2^+$ type structures with respect to their minimum energies. In Figure 9 are illustrated four reasonable geometrical configurations of interest for $BF_2H_2^+$. Results of the calculations are presented in Table IV. Energy differences are indicated by reference to structure I. These calculations are helpful only for comparison purposes and are not to be interpreted with quantitative accuracy. The B–F distances obtained appear to be abnormally long with respect to the B–F distances in BF_3 (1.30 Å). This is common to all the structures calculated. Structure I with the axis of the H_2 unit perpendicular to the principal symmetry axis was found to be more stable than structure II with the H–H axis coinciding with the symmetry axis. A similar result was obtained by Olah and coworkers for the BH_5 structure formed by joining an H_2 unit to BH_3.[13] In structures I and II the H–H distance is longer than that in H_2 but shorter than in H_2^+. This effect is typical of three-center terminal-bond structures calculated for CH_5^+ and BH_5. Structure IV, which was found to be the most stable of the structures tested, is about 1 eV more stable than structure I.

Discussion

Kinetic Analysis. The magnitude of the rate constants for the formation of the product ions in the present systems may be compared to that measured for the reaction of H_3^+ with H_2 under nearly identical conditions [$k_3 = (2.16 \pm 0.102) \times 10^{-28}$ cm^3/(molecule sec)[2] at 86°K].[15] Normally it would be expected that the rate constants for the processes of current interest are larger than that for H_5^+ formation due to the increased size of BF_3H^+, BF_2^+, and $BF_2H_2^+$ ions with respect to H_3^+, consequently leading to larger reactive cross sections. Indeed only the rate constant for $BF_2{\cdot}H_2^+$ formation reflects this anticipated effect. Recent developments based on a previous postulation of a "ballistic" theory of fragmentation have shown by comparison with experimental results that dependence on internal structure for bimolecular processes reduces rate coefficients.[16] Consideration of the "path degeneracy" taken as the number of equivalent sites for attack on the neutral molecule improves the prediction obtained over that of the Langevin theory for estimation of reaction rates. Although this treatment does not include simple three-body reactions in presentation, application of the concept of "path degeneracy" may indeed give suitable explanation for the lower rate constants observed for $BF_3H{\cdot}H_2^+$ and $BF_2H_2{\cdot}H_2^+$ formation. Presumably the ions H_3^+ and BF_2^+ will have a substantially larger number of avenues of attack for initial complex formation than the less symmetrical BF_3H^+ and $BF_2H_2^+$ species. This may indeed in large measure provide explanation of the reduction of the rate constants involving these species.

Throughout, two distinct representations have been employed to indicate structural prejudice for the $BF_2H_2^+$ type species. The form $BF_2H_2^+$ has been used to indicate that ion formed by protonation of HBF_2 and the form $BF_2{\cdot}H_2^+$ has been used for that species generated by H_2 addition to BF_2^+ in the presence of a third body. On the basis of the physical information this distinction appears to be quite reasonable. In general it would not be expected that the rate constant for the process

$$BF_2{\cdot}H_2^+ + 2H_2 \rightarrow BF_2{\cdot}2H_2^+ + H_2 \qquad (20)$$

would be the same as that for reaction 16. In fact analysis of rate data shown in the lower part of Figure 5 indicates that reaction 20 has approximately the same rate constant as reaction 16 within the experimental uncertainties.

Thermochemical Analysis. The structure calculations for the $BF_2H_2^+$ type species indicate that there may be several isomers of this ion of comparable stability. A species with the symmetry of structure IV is probably formed by proton addition to HBF_2 by reaction 12 at ambient temperatures, while structure I, which does not require formation of the H–F bond, is probably more readily formed through the condensation reaction (eq 15) at low temperatures. Proton transfer from H_3^+ to BF_3 almost certainly results in proton attachment at a fluorine atom. It may be noted that BF_3H^+ is isoelectronic with BF_2OH, which has a planar configuration.[17] If proton attachment occurs at the same functional group in both HBF_2 and BF_3 the proton affinities should be nearly identical. The present measurements do not have sufficient precision to determine this exactly.

It is noted that for the species with the empirical formula $BF_2H_{2m}^+$, the maximum value of m observed is 2. This implies an effective coordination of four groups to boron, with at least two possible isomeric structures, **1a** and **1b**. The question of

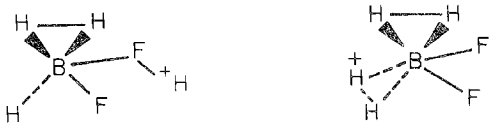

1a **1b**

whether different isomers of the forms $BF_2{\cdot}2H_2^+$ and $BF_2H_2{\cdot}H_2^+$ are formed in these systems by different pathways is in part answered by physical evidence and calculations. It would appear that the species formed by addition of H_2 to protonated HBF_2 and that formed by two consecutive H_2 additions to BF_2^+ are distinguishable isomers that cannot be interconverted through a reversible mechanism.

Acknowledgment. We are grateful for support by the Army Research Office, Durham, N.C., and by the National Science Foundation (Grant GH 33637) through the Materials Science Center, Cornell University. We wish to thank Mr. Gary Sahagian for assistance with theoretical calculations.

Registry No. BF_3, 7637-07-2; HBF_2, 13709-83-6; H_2, 1333-74-0; D_2, 7782-39-0.

References and Notes

(1) J. J. Solomon and R. F. Porter, *J. Amer. Chem. Soc.*, **94**, 1443 (1972); R. C. Pierce and R. F. Porter, *ibid.*, **95**, 3849 (1973).
(2) R. C. Pierce and R. F. Porter, *J. Amer. Chem. Soc.*, **95**, 3849 (1973).
(3) R. F. Porter and S. K. Wason, *J. Phys. Chem.*, **69**, 2208 (1965).
(4) L. Barton, F. Grimm, and R. F. Porter, *Inorg. Chem.*, **5**, 2076 (1966).
(5) J. L. Franklin, J. G. Dillard, H. M. Rosenstock, J. T. Herron, K. Draxl, and F. H. Field, *Nat. Stand. Ref. Data Ser., Nat. Bur. Stand.*, **No. 26**, 1969.
(6) "JANAF Thermochemical Tables," *Nat. Stand. Ref. Data Ser., Nat. Bur. Stand.*, **No. 37** (1971).
(7) M. T. Bowers, W. J. Chesnavich, and W. T. Huntress, Jr., *Int. J. Mass Spectrom. Ion Phys.*, **12**, 357 (1973).
(8) F. C. Fehsenfeld, A. L. Schmeltekopf, and E. E. Ferguson, *J. Chem. Phys.*, **46**, 2802 (1967).
(9) G. H. Wamis, *Bell Syst. Tech. J.*, **32**, 170 (1953).
(10) W. A. Chupka and J. Berkowitz, *J. Chem. Phys.*, **54**, 4526 (1971).
(11) J. A. Pople and G. A. Segal, *J. Chem. Phys.*, **44**, 3289 (1966).
(12) W. A. Lanthan, W. J. Hehre, and J. A. Pople, *J. Amer. Chem. Soc.*, **93**, 808 (1971).
(13) G. A. Olah, P. W. Westerman, Y. K. Mo, and G. Klopman, *J. Amer. Chem. Soc.*, **94**, 7859 (1972).
(14) H. Levy and L. O. Brockway, *J. Amer. Chem. Soc.*, **59**, 2085 (1937).
(15) R. C. Pierce and R. F. Porter, *Chem. Phys. Lett.*, **23**, 608 (1973).
(16) P. F. Knewstubb, *Int. J. Mass Spectrom. Ion Phys.*, **10**, 371 (1973).
(17) H. Takeo and R. F. Curl, *J. Chem. Phys.*, **56**, 4314 (1971).

Contribution from the Department of Chemistry, University of Colorado, Boulder, Colorado 80302

Oxidation of Trimethylgermylphosphine and Bis(phosphino)dimethylgermane[1]

ALAN R. DAHL and ARLAN D. NORMAN[2*]

Received August 15, 1974 AIC40584S

The phosphinogermanes $(CH_3)_3GePH_2$ and $(CH_3)_2Ge(PH_2)_2$ react rapidly with gaseous O_2 to yield a mixture of oxidation products. From these reactions, the new phosphonoxygermoxane compounds $[(CH_3)_3GeO]_2P(O)H$ and $[(CH_3)_2GeOP(O)HO]_2$ have been isolated. Spectral data allow the compounds to be characterized as phosphonates. An alternate synthesis of $[(CH_3)_2GeOP(O)HO]_2$ from the reaction of H_3PO_3 and $(CH_3)_2Ge(PH_2)_2$ is reported.

Introduction

Redistribution reactions on the phosphorus atoms of bis(phosphino)dialkylgermanes result in the formation of novel germanium–phosphorus condensed products.[3,4] These redistribution reactions were observed to be catalyzed by trace quantities of oxidation products of the bis(phosphino)dialkylgermanes. Since catalyzed redistribution reactions might have application to the syntheses of a wide variety of new compounds, characterization of the oxidation products becomes of paramount importance. Although the oxidation products of tertiary phosphines containing covalently bonded silicon, germanium, tin, and lead have been studied,[5-7] the O_2 oxidation of primary or secondary group IV moiety substituted phosphines has not been examined. We report the first study of this type.

Experimental Section

Apparatus, Materials, and Techniques. All work was carried out in a standard high-vacuum system.[8] Melting points were obtained in sealed capillaries. Infrared spectra were obtained in the range 4000–400 cm^{-1} on a Perkin-Elmer Model 337G spectrometer on neat samples or samples pressed between KBr plates. Proton nmr spectra were obtained at 60.0 and 100.0 MHz using Varian A-60A and HA-100 spectrometers. Phosphorus-31 nmr spectra were obtained at 40.5 MHz using a Varian HA-100 equipped with standard probe and radiofrequency unit accessories. Mass spectra were obtained using Varian MAT CH-5 and CH-7 spectrometers operating at an ionizing voltage of 70 eV. Mass spectral envelopes for polygermanium -containing molecular species[9] were calculated essentially as described previously.[10] The isotopic distribution patterns centered at m/e 146 and 218 are diagnostic for Ge_2- and Ge_3-containing species, respectively.

The $(CH_3)_3GePH_2$ and $(CH_3)_2Ge(PH_2)_2$ were prepared and purified as described previously.[11] Reagent grade anhydrous phosphorous acid (Baker Chemical Co.), 95% ethanol, and chloroform were used without further purification. Oxygen (Matheson Co.) was passed through a −196° trap prior to use.

Reactions with O_2. (A) $(CH_3)_3GePH_2$. Typically, 3.5 mmol of $(CH_3)_3GePH_2$ and 10 ml of chloroform were condensed into a 500-ml round-bottom flask. The flask was connected to the vacuum line at a side-arm U tube on the flask. The reaction bulb was warmed to −45° and 5–10 Torr of gaseous oxygen was admitted. After *ca.* 1 hr, additional oxygen was bled slowly into the reactor. Bursts of flame occurred as the oxygen pressure reached *ca.* 20 Torr. *Caution! Care should be taken to add the oxygen slowly, since an excessive burning rate could cause overheating and a subsequent explosion.* Oxygen was added in intervals of 5–10 min until bursts of flame no longer occurred. During the reaction yellow-orange solid deposited on the walls of the reactor. The reactor was heated to 150° and reaction materials were removed through the side-arm U trap maintained at −30°. Chloroform and a trace of PH_3 (confirmed by ir spectrum)[12] passed the −30° trap. The side arm was reattached to a double U-tube sublimation tube. The material in the side arm was heated to 100–110° and allowed to distil into the two traps, maintained at −30° (fraction I) and 0° (fraction II). Repeated distillation of fraction II resulted in a 10% yield of pure $[(CH_3)_3GeO]_2P(O)H$. *Anal.* Calcd for $C_6H_{19}Ge_2O_3P$: C, 19.09; H, 5.07. Found: C, 19.31; H, 5.01.

$[(CH_3)_3GeO]_2P(O)H$ shows infrared absorptions at 3390 (m), 2963 (m), 2899 (m), 2778 (vw), 2331 (s), 1639 (w), 1412 (m), 1227 (vs), 1149 (s), 1094 (m, sh), 1010 (vs), 830 (vs), 769 (w, sh), 671 (w), 627 (s), 577 (m), and 478 (m) cm^{-1}. The most intense peaks in the ten most intense mass spectral envelopes occur at m/e (relative intensities in parentheses) 316 (8.9), 301 (29.0), 183 (13.1), 167 (5.6), 137 (7.9), 119 (100.0), 105 (12.6), and 89 (18.2). The parent envelope centered at m/e 316 is, within experimental error, superimposable with that expected for a molecule containing two Ge atoms. Proton and ^{31}P nuclear magnetic resonance data are given in Table I.

Table I. Nuclear Magnetic Resonance Spectral Data

Measurement	$[(CH_3)_3GeO]_2P(O)H$	$[(CH_3)_2GeOP(O)HO]_2$
	^1H Nmr Data[a]	
$\delta(CH_3)$[b]	−0.52 ± 0.03	−1.02 ± 0.03
$\delta(PH)$[b]	−6.75 ± 0.03	−6.80 ± 0.03
$^1J(PH)$[c]	681 ± 2	708 ± 3
	^{31}P Nmr Data[a]	
$\delta(P)$[d]	−1 ± 2	7 ± 2

[a] Obtained on 10–20% (by volume) solutions in $CHCl_3$. [b] Chemical shifts in ppm relative to internal $(CH_3)_4Si$. [c] Coupling constants in Hz. [d] Chemical shift in ppm relative to external 85% H_3PO_4.

Fraction I, upon repeated distillation, could not be separated completely. Mass spectral analyses showed it to consist predominantly of a material whose parent molecular ion mass spectral envelope occurred at m/e 183, along with a small quantity of $[(CH_3)_3GeO]_2P(O)H$. The most intense peak in each of the eight most intense envelopes for this material occurred at m/e (relative intensity in